Unveiling excited-state chirality of ninaphthols by femtosecond circular dichroism and quantum chemical calculations

Marco Schmid, Lara Martinez-Fernandez, Dimitra Markovitsi, Fabrizio Santoro, François Hache, Roberto Improta, Pascale Changenet

THE JOURNAL OF PHYSICAL CHEMISTRY Letters

Letter

Cite This: J. Phys. Chem. Lett. 2019, 10, 4089−4094

pubs.acs.org/JPCL

Unveiling Excited-State Chirality of Binaphthols by Femtosecond Circular Dichroism and Quantum Chemical Calculations

Marco Schmid,[†] Lara Martinez-Fernandez,[§,∥] Dimitra Markovitsi,[§] Fabrizio Santoro,[#] François Hache,[†] Roberto Improta,*[,§,‡] and Pascale Changenet*[,†]

[†]Laboratoire d'Optique et Biosciences, CNRS, INSERM, Ecole Polytechnique, Institut Polytechnique de Paris, 91128 Palaiseau Cedex, France

[§]LIDYL, CEA, CNRS, Université Paris-Saclay, F-91191 Gif-sur-Yvette, France

[#]Consiglio Nazionale delle Ricerche, Istituto di Chimica dei Composti Organometallici, SS di Pisa, Area della Ricerca, via G. Moruzzi 1, I-56124 Pisa, Italy

[‡]Istituto Biostrutture e Bioimmagini, Consiglio Nazionale delle Ricerche, Via Mezzocannone 16, I-80134 Napoli, Italy

[∥]Departamento de Química, Facultad de Ciencias, Modúlo13, Universidad Autónoma de Madrid, Campus de Excelencia UAM-CSIC, Cantoblanco, 28049 Madrid, Spain

Supporting Information

ABSTRACT: Time-resolved circular dichroism (TR-CD) is a powerful tool for probing conformational dynamics of biomolecules over large time scales that are crucial for establishing their structure−function relationship. However, such experiments, notably in the femtosecond regime, remain challenging due to their extremely weak signals, prone to polarization artifacts. By using binol and two bridged derivatives (PL1 and PL2) as chiral prototypes, we present here the first comprehensive study of this type in the middle UV, combining femtosecond TR-CD and quantum mechanical calculations (TD-DFT). We show that excitation of the three compounds induces large variations of their transient CD signals, in sharp contrast to those of their achiral transient absorption. We demonstrate that these variations arise from both the alteration of the electronic distribution and the dihedral angle in the excited state. These results highlight the great sensitivity of TR-CD detection to signals hardly accessible to achiral transient absorption.

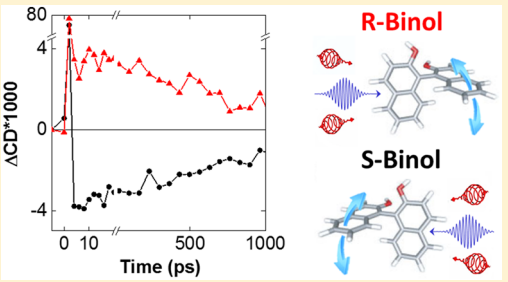

Circular dichroism (CD) is a noninvasive tool for investigating the three-dimensional structure of proteins and DNA in solution.[1] An extension to time-resolved measurements provides interesting perspectives for probing their conformational dynamics over large time scales.[2,3] However, CD measurements at a very short time scale remain challenging due to extremely weak signals, prone to polarization artifacts, in particular, in the UV spectral domain.[4−12] So far, only a few examples of femtosecond CD measurements are reported in the literature, most of them being limited to proof-of-principle experiments.[5−8,10,13−16]

Herein, we present a comparative study of several chiral compounds in different solvents, below 250 nm, by femtosecond TR-CD spectroscopy. As models of chiral systems, we chose binol and two bridged derivatives, PL1 and PL2 (Scheme 1a). These 2,2′-homosubstituted 1,1′-binaphthyls are axial chiral compounds whose enantiomers are called atropoisomers and specified by the stereodescriptors P/M or R_a/S_a. These enantiomers can adopt three conformations, cisoid, orthogonal, or transoid, depending on the dihedral angle (θ) between the planes of their two aromatic subunits (Scheme 1b). Because binol chirality arises from the competition between steric hindrance (favoring orthogonal arrangements) and electronic coupling of the two aromatic subunits (favoring coplanar arrangements),[17−20] photoinduced changes of θ may significantly affect their chiroptical properties, as recently shown by one of us using femtosecond CD.[21] Besides conformational changes, TR-CD can also yield precise information about changes of their electronic structure after excitation. To address the delicate balance between those factors, we examined the role of the substituents and the solvent on the chiroptical responses of binols upon excitation. Our results are interpreted thanks to TD-DFT calculations in solution, using the M052X and CAM-B3LYP functionals and the PCM solvation model.

Figure 1 reports the static absorption, CD, and fluorescence spectra of (S_a)-binol, (R_a)-PL1, and (R_a)-PL2 in cyclohexane (Cx). The absorption spectra display three peaks associated with ^1L_b (S_1 the weakest, 328 nm), ^1L_a (S_2, 278 nm), and ^1B_b (S_3, 226 nm) electronic states according to the Platt notation.[18,20,21] Their similarity with those of 2-naphthol has been attributed to the weak interaction between the two

Received: April 3, 2019
Accepted: July 1, 2019
Published: July 1, 2019

DOI: 10.1021/acs.jpclett.9b00948
J. Phys. Chem. Lett. 2019, 10, 4089−4094

Scheme 1. Schematic Representations of (a) the Three Studied 2,2′-Homosubstituted 1,1′-Binaphthyl Compounds, (R_a)-Binol, (R_a)-PL1, and (R_a)-PL2, and (b) 1,1′-Binaphthyl Conformers

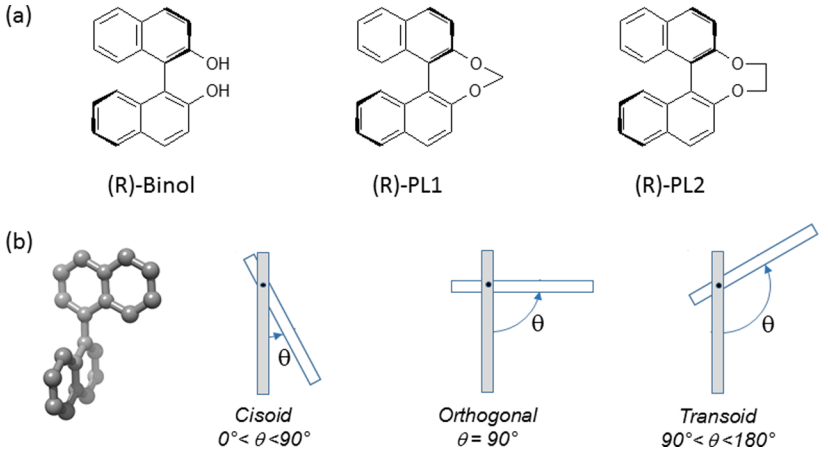

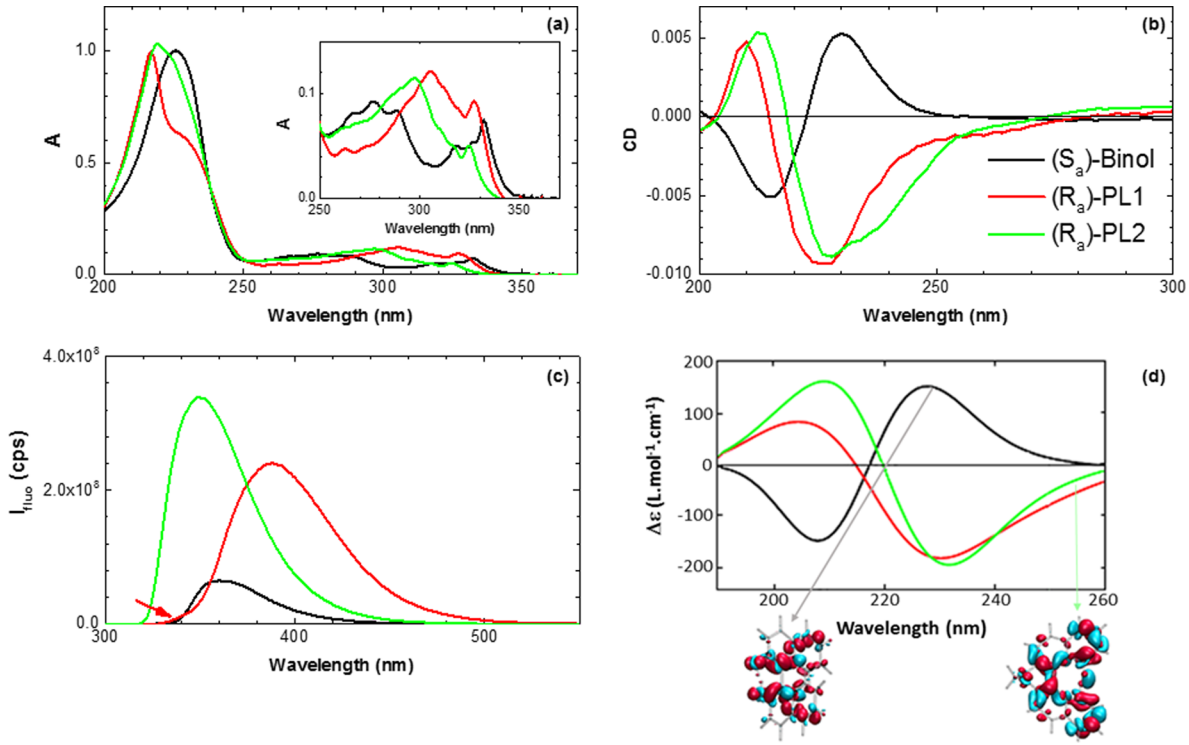

Figure 1. (a) Static absorption spectra, (b) corresponding static CD spectra in optical density (OD), and (c) fluorescence spectra of (S_a)-binol (black lines), (R_a)-PL1 (red lines), and (R_a)-PL2 (green lines) measured in cyclohexane (Cx). The relative fluorescence spectral areas are representative of the quantum yields. The red arrow indicates the small shoulder in the fluorescence of (R_a)-PL1. Excitation wavelength: λ = 290 nm. (d) Computed CD spectra in Cx at the PCM/TD-CAM-B3LYP/6-31+G(d,p)//PCM/TD-CAM-B3LYP/6-31G(d) level of theory at the S_0-min. The excited-state density differences ($S_n - S_0$) for the S_7 transition of (S_a)-binol and the S_6 transition of (R_a)-PL1 are also shown. Each transition has been convoluted with a Gaussian function (with a half-width half-maximum of 0.3 eV).

aromatic moieties.[22] Our quantum chemical calculations indeed predict that competition between resonance and steric hindrance, involving the two aromatic moieties, favors the quasi-orthogonal conformation in solution ($\theta \approx 90°$). However, the molecular structure of binol in the ground state is rather flexible, leading to a large distribution of conformations ranging between slightly cisoid to slightly transoid ones ($70 < \theta < 110°$) at room temperature (Figure S2 in the Supporting Information (SI)). We found that the mixing of ^1L_a and ^1L_b transitions is more important than that in 2-naphtol. We clearly recognize two ^1L_a excitons (one almost dark), two ^1L_b excitons (one dark), and two ^1B_b excitons, derived from the combination of ^1L_a, ^1L_b, and ^1B_b states of the 2-naphtol units (Table S1). The computed absorption spectra of binol are consistent with the experimental ones but overestimate the stability of the ^1L_a excitons.

The presence of the bridges induces a prominent bathochromic shift of the ^1L_a transition, concomitant to a hypsochromic shift of the ^1L_b transition, giving rise to one congested absorption band peaking at 305 and 297 nm, respectively, for (R_a)-PL1 and (R_a)-PL2. Those shifts stem from the steric constraint imposed by the bridges that

DOI: 10.1021/acs.jpclett.9b00948
J. Phys. Chem. Lett. 2019, 10, 4089−4094

provokes a substantial deviation of the oxygen substituents from the plane of the two aromatic rings and reduces the delocalization of the oxygen lone pairs.[23] The bridges considerably reduce the degree of freedom of the dihedral angle. Consequently (R_a)-PL1 and (R_a)-PL2 exhibit a unique cisoid conformation in the ground state, with θ being equal to −49 and −61°, respectively (Figure S5).

The static CD spectrum (CD_{GS}) of binol displays a characteristic excitonic bisignate in the 200−250 nm spectral region. It is well-established from simple classical models of coupled oscillators that the amplitude and the sign of this bisignate strongly depend on θ.[17,19] In this context, the largest amplitude of the Cotton effect observed in (R_a)-PL1 is consistent with its small θ. It is clear from our calculations (Figure S6) that the large distribution of θ in (S_a)-binol also significantly contributes to this difference. The origin of the CD bisignate arises from the interactions of the two 2-naphthol units derived from the excitonic coupling of their ^1B_b transitions. As illustrated in Figure 1d, these interactions lead to an additional shoulder in the red edge of (R_a)-PL1 and (R_a)-PL2 bisignate that pertains to an inter-ring charge transfer transition delocalized over the whole molecule derived from the HOMO → LUMO transitions of the 2-naphthol moieties.

Besides CD, fluorescence spectroscopy can provide valuable information about the nature of the excited state of biaryl compounds.[24−28] (S_a)-binol, (R_a)-PL1, and (R_a)-PL2 in Cx (Figure 1c) exhibit a broad fluorescence spectrum with a Stokes shift higher than 2700 cm^{-1}. Such a behavior, which was also reported for the achiral 1,1′-binaphthyl, has been attributed to the significant change of θ upon excitation.[29] As shown by our calculations, while such interpretation is also valid for (S_a)-binol and (R_a)-PL2, it is inappropriate for (R_a)-PL1 for which large-amplitude motions are not expected. In this case, we clearly observe a dual fluorescence (Figure 1c), indicating emission from two distinct excited states. This peculiar behavior can be explained by the inversion of ^1L_a and ^1L_b states after excitation. Such an inversion has been reported for other aromatic systems, as, for example, 1-naphthol and indole derivatives.[30,31] According to this scenario, the blue-edged fluorescence band (<350 nm), clearly distinguishable for (R_a)-PL1, can be attributed to emission from the lowest ^1L_b state and the red-edged band (>380 nm) to the emission of the ^1L_a state. We infer here a predominant role of θ in the inversion of ^1L_a and ^1L_b states that also appears in the absorption spectra of the three studied compounds, where the relative energy between the two ^1L transitions is strongly diminished by the bridges.

To access the chiroptical changes of binols upon excitation, we recorded their TR-CD signals at 234 nm, i.e., in the spectral region corresponding to the largest amplitude of their static CD signals in absolute value. Due to the strong energetic pump, both the measured achiral differential absorbance (ΔA) and the differential CD signals (ΔCD) exhibit a strong peak around the time zero (Figure S8). This peak, which is also observed for the neat solvent (Figure S9), results from two-photon absorption (TPA) by the solvent and increases the uncertainty of the TR-CD measurements on the subpicosecond time scale. Typical ΔCD kinetics measured after TPA in Cx, ethanol (EtOH), and ethylene glycol (EtG) (Table S4) are presented in Figure 2. They correspond to the ground-state bleaching due to the dominant contribution of CD_{GS}. In other words, UV excitation induces a decrease of the CD in the excited state (CD_{ES}) in absolute value, i.e., $|CD_{ES}| < |CD_{GS}|$. At

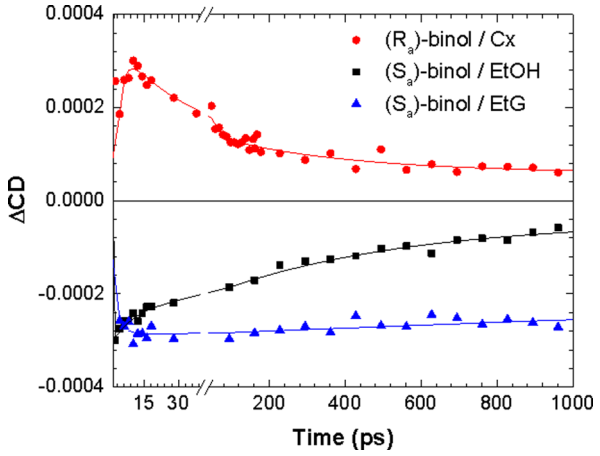

Figure 2. Comparison of the normalized TR-CD changes in OD measured after 1 ps at 234 nm for (S_a)-binol in ethanol (EtOH) and ethylene glycol (EtG) and (R_a)-binol in Cx. Solid lines represent the individual fits of the experimental data. Excitation: 266 nm.

the probe wavelength, CD_{GS} of (S_a)-binol in EtOH being positive, the depletion of the ground-state population induced by excitation appears as a negative signal. Conversely, the CD_{GS} signal of (R_a)-binol in Cx being negative, the depletion of the ground-state population upon excitation appears as a positive signal. Importantly, the measured ΔCD kinetics are found to be significantly faster than those of achiral ΔA (Figure S10). Because CD_{GS} is expected to be constant, we can thus deduce that the observed ΔCD kinetics mainly originates from the temporal variation of CD_{ES}.

The ΔCD kinetics of binol were fitted with a sum of two or three exponentials and a step function with an amplitude of less than 10% (Table 1). This step function accounts for the residual contribution of the cell birefringence (see the SI). The kinetics measured for Cx and EtG solutions involves two distinct stages associated with amplitudes of different signs. The first stage (τ_1) indicates that immediately after excitation CD_{ES} is similar to CD_{GS} and then gradually changes within a few picoseconds. Those changes are consistent with a decrease of $|CD_{ES}|$.

On longer time scales, the TR-CD signals obtained for fluid Cx and EtOH solutions exhibit a biphasic behavior with average lifetimes of 136 and 400 ps, respectively. In the viscous EtG, kinetics are monoexponential and markedly slower (τ_2 = 8 ns). They are consistent with an increase of $|CD_{ES}|$. The remarkable slowdown of the ΔCD kinetics in the viscous EtG is consistent with a large-amplitude motion of the aromatic moieties of binol. Our geometry optimizations (potential energy surfaces, PESs) illustrated in Figure 3 indeed predict large changes of θ of ca. ±40°, toward a more planar geometry, especially for ^1L_a-derived states. Both transoid and cisoid conformations can be populated from the large conformational distribution of the ground state of binol, the transoid conformation being more stable than the cisoid one.

In order to characterize the substituent effect on the chiroptical properties of binols after excitation, we performed TR-CD measurements on (R_a)-PL1 and (R_a)-PL2. Figure 4 compares typical signals recorded for Cx, EtOH, and EtG solutions. Like (R_a)-binol in Cx solutions, both bridged compounds exhibit positive TR-CD signals, consistent with $|CD_{ES}| < |CD_{GS}|$. They were fitted with the sum of one or two

DOI: 10.1021/acs.jpclett.9b00948
J. Phys. Chem. Lett. 2019, 10, 4089−4094

Table 1. Time Constants and Relative Percentage Amplitudes Obtained from the Individual Fits of the ΔCD Changes of (S_a)- and (R_a)-Binols at 234 nm

binols	τ_1 (a_1)	τ_2 (a_2)	τ_3 (a_3)	step
(R_a)-binol/Cx	2 ± 1 ps (−0.5)	29 ± 8 ps (0.28)	368 ± 200 ps (0.13)	0.09
(S_a)-binol/EtOH		18 ± 8 ps (−0.31)	570 ± 190 ps (−0.69)	
(S_a)-binol/EtG	3 ± 2 ps (0.22)	8 ± 2 ns (−0.78)		

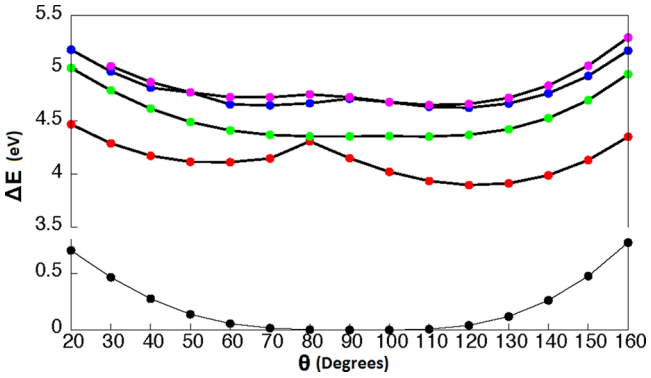

Figure 3. Relative energy of the five lowest electronic states of (S_a)-binol for different values of the dihedral angle (θ), computed at the PCM/TD-CAM-B3LYP/6-31G(d) level of theory: S_0 PES in black, S_1 (bright ^1L_a-derived exciton state) in red, S_2 (dark ^1L_a-derived exciton state) in green, S_3 (bright ^1L_b-derived exciton state) in blue, and S_4 (dark ^1L_b-derived exciton state) in pink.

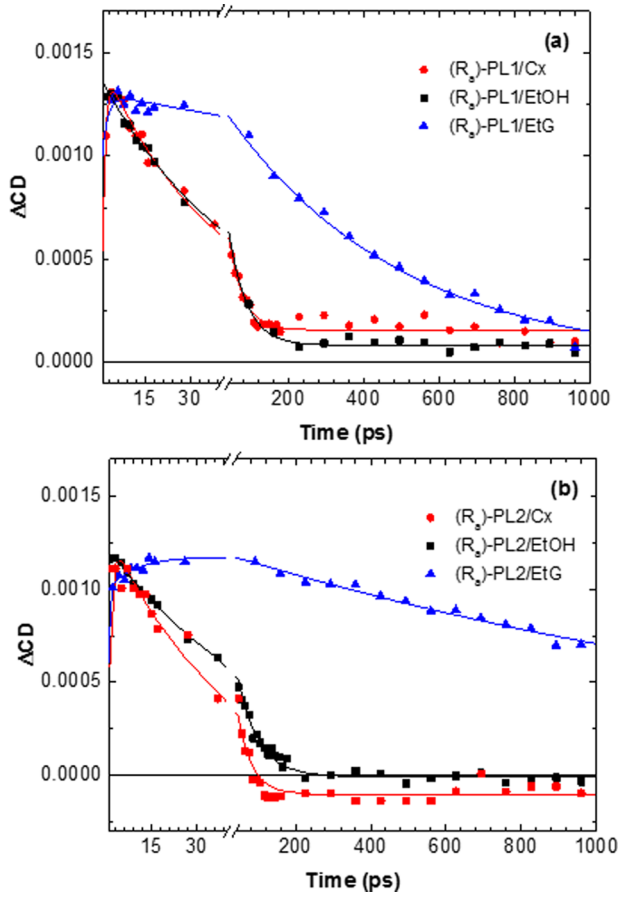

Figure 4. Comparison of the normalized TR-CD changes in OD measured at 234 nm for (R_a)-PL1 (a) and (R_a)-PL2 (b) in Cx, EtOH, and EtG. Solid lines represent the individual fits of the experimental data. Excitation: 266 nm.

exponential functions and a step function accounting for the cell birefringence artifact (Table 2).

Table 2. Time Constants and Their Relative Amplitudes Obtained from the Individual Fits of the ΔCD Changes of (R_a)-PL1 and (R_a)-PL2 at 234 nm

	τ_1 (a_1)	τ_2 (a_2)	step
PL1/Cx	0.9 ± 0.7 ps (−0.33)	38 ± 2 ps (0.60)	(0.07)
PL1/EtOH		48 ± 2 ps (0.94)	(0.06)
PL1/EtG	1.5 ± 0.5 ps (−0.50)	465 ± 11 ps (0.50)	
PL2/Cx		43 ± 3 ps (0.93)	(−0.07)
PL2/EtOH		55 ± 1 ps (1)	
PL2/EtG	10 ± 4 ps (−0.14)	1.9 ± 0.1 ns (0.86)	

A two-step behavior, i.e., a rise of a few picoseconds followed by an exponential decay, could be resolved in the TR-CD signals of both bridged compounds in EtG and (R_a)-PL1 in Cx. In all other cases, the ΔCD decays are monoexponential. As in the case of binol, these kinetics are much faster than those of achiral Δ*A* (Figure S11). We therefore attribute them to the temporal increase of $|CD_{ES}|$. Interestingly, both bridged compounds in fluid Cx and EtOH exhibit decays of ca. 40−50 ps, while in the viscous EtG, the decays are slower by more than 1 order of magnitude, suggesting the implication of structural changes in the excited state. In order to get further insight into those changes, we compared the TR-CD signals of (R_a)-PL1 and (R_a)-PL2 with those of binol. As a general trend, we observed that their ΔCD kinetics are faster. In particular, a less pronounced effect of the solvent viscosity is observed on the ΔCD kinetics of the bridged derivatives, giving support to smaller structural changes. This is in line with our calculations that predicted small variations of θ equal to −4 and −14°, for (R_a)-PL1 and (R_a)-PL2, respectively.

As a last step of our analysis, we computed CD_{ES} spectra associated with the four lowest energy excited states of (S_a)-binol at some representative stationary points of their PES using quadratic response theory calculations (see the SI). It has to be pointed out that a direct comparison with our experiments is not possible because it would require calculations of all of the rotatory strength between the excited states in an energy window of 10 eV (i.e., for more than 100 excited states), well beyond the ionization limit. We thus limit our analysis to the energy window up to ∼8 eV, i.e., ∼3 eV above the considered excited states, where our TD-DFT calculations are more reliable. According to our calculations, each excited state exhibits distinct CD signals with different dependence on θ and the considered energy window (i.e., the probe wavelength; see the SI). This result, together with the strong vibronic coupling between the different excited states evidenced by our calculations and the possible role of CT states, shows that a simple exciton model, based on the behavior of the GS spectra, cannot provide a reliable interpretative framework.

DOI: 10.1021/acs.jpclett.9b00948
J. Phys. Chem. Lett. 2019, 10, 4089−4094

The CD_{ES} signals depend remarkably on the considered excited state. A smaller, albeit, clear dependence on the geometry is also found (Figure S14). In particular, the computed signals are much larger for the B-symmetry states corresponding to the bright L_a-1 and L_b-1 exciton states than those for A-symmetry states corresponding to the dark L_a-2 and L_b-2 exciton states. In addition, exciton localization induces a significant decrease of the CD_{ES} amplitude. Finally, the B-symmetry states exhibit larger signals in their ground-state geometry and in their cisoid minima than their transoid ones.

A combination of these computations and our experimental observations provides a qualitative picture of the complex photoactivated dynamics and the TR-CD signals of binols. In the first picosecond, CD_{ES} remains similar to CD_{GS}. Subsequently, we observe a decrease of the CD signal, which can be attributed to the decay to transoid excited-state minima associated with the trapping in partially localized minima. Afterward, a steep increase of the signal is observed, suggesting a significant change in the nature of the excited-state population. Actually, both our calculations and our fluorescence spectra provide several arguments in favor of the inversion between ^1L_a and ^1L_b states, with population transfer to the ^1L_a exciton. First, the bright ^1L_a excitons are more sensitive to the variations of θ and further stabilized compared to the other excited states. Second, the ^1L_b states are characterized by a weaker exciton coupling that the ^1L_a states, leading to partial localization of the excitation on one ring after excitation. Consequently, our geometry optimizations indicate that the ^1L_a exciton minimum is the most stable one. Depopulation of the partially localized pseudominima can also contribute to the relative increase of the CD signal.

Vibronic interactions ruling these population transfers, e.g., $^1L_b \rightarrow {}^1L_a$ or localized → delocalized minima, are obviously modulated by the structural degrees of freedom, with θ playing an important role. This conclusion is supported by the almost constant TR-CD signal observed for binol in EtG. In this solvent, most of the molecules are expected to be frozen in a "pseudo-perpendicular" arrangement, preventing the population transfer processes described above. (R_a)-PL1 and (R_a)-PL2 are instead constrained in a cisoid conformation in all solvents, for which the vibronic coupling between ^1L states coupling is significantly higher, as shown by their absorption spectra. This result is in line with the faster kinetics of their TR-CD signals with respect to those of binol, observed in all of the solvents including EtG. The ΔCD kinetics of (R_a)-PL1 in EtG is indeed comparable to that of binol in EtOH. On the other hand, the similar qualitative behavior observed for the three studied compounds provides a strong indication that, although important, θ is not the only structural parameter affecting the vibronic coupling in biaryls. In this respect, it is noteworthy that the dual fluorescence of (R_a)-PL1 indicates the inversion of $^1L_a/^1L_b$ states despite limited changes.

Regarding the solvent effects, the shorter average lifetime of the ΔCD kinetics of binol observed in Cx with respect to those in EtOH indicates a marked effect of the solvent proticity on the excited-state relaxation. The propensity of the binol hydroxyl groups to form hydrogen bonds with EtOH induces a net deceleration of the conformational changes by more than 1 order of magnitude with respect to 1,1-binaphthyl, i.e., 400 vs 12 ps.[32] For (R_a)-PL1 and (R_a)-PL2, there is no significant effect of the solvent proticity on the TR-CD, providing evidence that the presence of the bridges prevents specific interactions of the oxygen atoms with protic solvents.

In conclusion, we presented the first comprehensive femtosecond TR-CD study of binol and two bridged derivatives and examined the solvent effect. Upon excitation, we observed significant changes in the TR-CD signals caused by the CD_{ES} dynamics. A combination of TR-CD, fluorescence spectroscopy, and quantum chemical calculations brought evidence that those effects stem from the intricate changes of the electronic structure and the conformation of biaryls upon excitation. In a more general way, these experiments highlight the great potential of TR-CD detection with respect to classical achiral transient absorption to detect both electronic and conformational changes of excited states.

■ ASSOCIATED CONTENT

Supporting Information

The Supporting Information is available free of charge on the ACS Publications website at DOI: 10.1021/acs.jpclett.9b00948.

Experimental and computational details, steady-state fluorescence in ethanol and ethylene glycol, additional time-resolved absorption and CD measurements, and excited-state CD calculations (PDF)

■ AUTHOR INFORMATION

Corresponding Authors

*E-mail: pascale.changenet-barret@polytechnique.edu.
*E-mail: robimp@unina.it.

ORCID

Dimitra Markovitsi: 0000-0002-2726-305X
Fabrizio Santoro: 0000-0003-4402-2685
Roberto Improta: 0000-0003-1004-195X
Pascale Changenet: 0000-0002-5874-6249

Notes

The authors declare no competing financial interest.

■ ACKNOWLEDGMENTS

The authors acknowledge financial support from the Agence Nationale de la Recherche (ANR-12-BS04-0018 Dynachir) and labex PALM (QUADfold and OSPEG projects, ANR-10-LABX-0039-PALM). R.I. acknowledges support from Université Paris Saclay-programme D'Alembert 2016, no 10751. M.S. gratefully acknowledges support from the Triangle de la Physique. F.H. and P.C. wish to express their gratitude to L. Guy from ENS at Lyon and S. Guy from ILM at Lyon for providing them the bridged binol derivatives. F.S. thanks Dr. A. Rizzo and S. Coriani for useful discussions on excited-state CD calculations.

■ REFERENCES

(1) Fasman, G. D. *Circular Dichroism and the conformational analysis of biomolecules*; Plenum Press: New York, 1996.
(2) Lewis, J. W.; Goldbeck, R. A.; Kliger, D. S.; Xie, X.; Dunn, R. C.; Simon, J. D. Time-resolved circular dichroism spectroscopy: Experiment, theory, and applications to biological systems. *J. Phys. Chem.* **1992**, *96*, 5243−5254.
(3) Meyer-Ilse, J.; Akimov, D.; Dietzek, B. Recent advances in ultrafast time-resolved chirality measurements: perpective and outlook. *Laser Photonics Rev.* **2013**, *7*, 495−505.

DOI: 10.1021/acs.jpclett.9b00948
J. Phys. Chem. Lett. 2019, 10, 4089−4094

(4) Chen, E.; Goldbeck, R. A.; Kliger, D. S. Nanosecond time-resolved polarization spectroscopies: Tools for probing protein reaction mechanisms. *Methods* **2010**, *52*, 3−11.
(5) Hache, F. Application of time-resolved circular dichroism to the study of conformational changes in photochemical and photobiological processes. *J. Photochem. Photobiol., A* **2009**, *204*, 137−144.
(6) Hiramatsu, K.; Nagata, T. Broadband and ultrasensitive femtosecond time-resolved circular dichroism spectroscopy. *J. Chem. Phys.* **2015**, *143*, 121102.
(7) Mangot, L.; Taupier, G.; Romeo, M.; Boeglin, A.; Cregut, O.; Dorkenoo, K. D. H. Broadband transient dichroism spectroscopy in chiral molecules. *Opt. Lett.* **2010**, *35*, 381−383.
(8) Meyer-Ilse, J.; Akimov, D.; Dietzek, B. Ultrafast Circular Dichroism Study of the Ring Opening of 7-Dehydrocholesterol. *J. Phys. Chem. Lett.* **2012**, *3*, 182−185.
(9) Niezborala, C.; Hache, F. Measuring the dynamics of circular dichroism in a pump-probe experiment with a Babinet-Soleil compensator. *J. Opt. Soc. Am. B* **2006**, *23*, 2418−2424.
(10) Trifonov, A.; Buchvarov, I.; Lohr, A.; Würthner, F.; Fiebig, T. Broadband femtosecond circular dichroism spectrometer with white-light polarization control. *Rev. Sci. Instrum.* **2010**, *81*, 043104.
(11) Xie, X.; Simon, J. D. Picosecond time-resolved circular dichroism spectroscopy: experimental details and applications. *Rev. Sci. Instrum.* **1989**, *60*, 2614−2627.
(12) Stadnytskyi, V.; Orf, G. S.; Blankenship, R. E.; Savikhin, S. Near shot-noise limited time-resolved circular dichroism pump-probe spectrometer. *Rev. Sci. Instrum.* **2018**, *89*, 033104.
(13) Fidler, A. F.; Singh, V. P.; Long, P. D.; Dahlberg, P. D.; Engel, G. S. Dynamic localization of electronic excitation in photosynthetic complexes revealed with chiral two-dimensional spectroscopy. *Nat. Commun.* **2014**, *5*, 3286.
(14) Niezborala, C.; Hache, F. Excited-State Absorption and Circular Dichroism of Ruthenium(II) Tris(phenanthroline) in the Ultraviolet Region. *J. Phys. Chem. A* **2007**, *111*, 7732−7735.
(15) Mendonça, L.; Hache, F.; Changenet-Barret, P.; Plaza, P.; Chosrowjan, H.; Taniguchi, S.; Imamoto, Y. Ultrafast Carbonyl Motion of the Photoactive Yellow Protein Chromophore Probed by Femtosecond Circular Dichroism. *J. Am. Chem. Soc.* **2013**, *135*, 14637−14643.
(16) Oppermann, M.; Bauer, B.; Rossi, T.; Zinna, F.; Helbing, J.; Lacour, J.; Chergui, M. Ultrafast broadband circular dichroism in the deep ultraviolet. *Optica* **2019**, *6*, 56−60.
(17) Mason, S. F.; Seal, R. H.; Roberts, D. R. Optical Activity in the Byaryl Series. *Tetrahedron* **1974**, *30*, 1671−1681.
(18) Rosini, C.; Rosati, I.; Spada, G. P. A Conformational Analysis of Mono and Dialkyl Ethers of 2,2'-Dihydroxy-1,1'-binaphthalene by Circular Dichroism Spectroscopy and Cholesteric Induction in Nematic Liquid Crystals. *Chirality* **1995**, *7*, 353−358.
(19) Di Bari, L.; Pescitelli, G.; Salvadori, P. Conformational Study of 2,2'-Homosubstituted 1,1'-Binaphthyls by Means of UV and CD Spectroscopy. *J. Am. Chem. Soc.* **1999**, *121*, 7998−8004.
(20) Li, Z.-y.; Chen, D.-m.; He, T.-j.; Liu, F.-c. UV Near-Resonance Raman Spectroscopic Study of 1,1'-Bi-2-naphthol Solutions. *J. Phys. Chem. A* **2007**, *111*, 4767−4775.
(21) Niezborala, C.; Hache, F. Conformational changes in photoexcited (R)-(+)-1,1'-Bi-2-naphthol studied by time-resolved circular dichroism. *J. Am. Chem. Soc.* **2008**, *130*, 12783−12786.
(22) Lin, N.; Santoro, F.; Zhao, X.; Toro, C.; De Boni, L.; Hernandez, F. E.; Rizzo, A. Computational Challenges in Simulating and Analyzing Experimental Linear and Nonlinear Circular Dichroism Spectra. R-(+)-1,1 '-Bis(2-naphthol) as a Prototype Case. *J. Phys. Chem. B* **2011**, *115*, 811−824.
(23) Deussen, H.-J.; Hendrickx, E.; Boutton, C.; Krog, D.; Clays, K.; Bechgaard, K.; Persoons, A.; Bjørnholm, T. Novel Chiral Bis-dipolar 6,6′-Disubstituted Binaphthol Derivatives for Second-Order Nonlinear Optics: Synthesis and Linear and Nonlinear Optical Properties. *J. Am. Chem. Soc.* **1996**, *118*, 6841−6852.
(24) Hara, Y.; Nicol, M. F. Fluorescence spectra of 1,1'-binaphthyl and related compounds at high pressures. *Bull. Chem. Soc. Jpn.* **1978**, *51*, 1985−1987.
(25) Baraldi, I.; Bruni, M. C.; Caselli, M.; Ponterini, G. Rotamerism in 2,2'-Binaphthyl: A Study based on Fluorescence Analysis and CS-INDO/CI Calculations. *J. Chem. Soc., Faraday Trans. 2* **1989**, *85*, 65−74.
(26) Hochstrasser, R. M. The effect of intramolecular twisting on the emission spectra of hindered aromatic molecules part I. 1,1'-Binaphthyl. *Can. J. Chem.* **1961**, *39*, 459−470.
(27) Canonica, S.; Wild, U. P. Fluorescence Kinetics of 1, 1'-Binaphthyi in Fiuld and Rigid Solution. *J. Phys. Chem.* **1991**, *95*, 6535−6540.
(28) Marcelo, G.; de Francisco, R.; González-Álvarez, M. J.; Mendicuti, F. Fluorescence properties of (R)- and (S)-[1,1-binaphthalene]-2,2-diols solutions and their complexes with cyclodextrins in aqueous medium. *J. Photochem. Photobiol., A* **2008**, *200*, 114−125.
(29) Post, M. F. M.; Langelaar, J.; Van Voorst, J. D. W. The influence of the molecular conformation upon spectroscopic properties of 1,1'-binaphthyl. *Chem. Phys. Lett.* **1975**, *32*, 59−62.
(30) Messina, F.; Prémont-Schwarz, M.; Braem, O.; Xiao, D.; Batista, V. S.; Nibbering, E. T. J.; Chergui, M. Ultrafast Solvent-Assisted Electronic Level Crossing in 1-Naphthol. *Angew. Chem., Int. Ed.* **2013**, *52*, 6871−6875.
(31) Eftink, M. R.; Selvidge, L. A.; Callis, P. R.; Rehms, A. A. Photophysics of Indole Derivatives: Experimental Resolution of L_a and L_b Transitions and Comparison with Theory. *J. Phys. Chem.* **1990**, *94*, 3469−3479.
(32) Millar, D. P.; Eisenthal, K. B. Picosecond dynamics of barrier crossing in solution: A study of the conformational change of excited state 1,1'-binaphthyl. *J. Chem. Phys.* **1985**, *83*, 5076−5083.

DOI: 10.1021/acs.jpclett.9b00948
J. Phys. Chem. Lett. 2019, 10, 4089−4094